





# Detectable Molecular Features above Hydrocarbon Haze via Transmission Spectroscopy with *JWST*: Case Studies of GJ 1214b-, GJ 436b-, HD 97658b-, and Kepler-51b-like Planets

Yui Kawashima<sup>1,2,3</sup> , Renyu Hu<sup>4,5</sup>, and Masahiro Ikoma<sup>3,6</sup> 

<sup>1</sup>SRON Netherlands Institute for Space Research, Sorbonnelaan 2, 3584 CA Utrecht, The Netherlands; [y.kawashima@sron.nl](mailto:y.kawashima@sron.nl)

<sup>2</sup>Earth-Life Science Institute, Tokyo Institute of Technology 2-12-1-IE-1 Ookayama, Meguro-ku, Tokyo 152-8550, Japan

<sup>3</sup>Department of Earth and Planetary Science, Graduate School of Science, The University of Tokyo, 7-3-1 Hongo, Bunkyo-ku, Tokyo 113-0033, Japan

<sup>4</sup>Jet Propulsion Laboratory, California Institute of Technology, 4800 Oak Grove Drive, Pasadena, CA 91109, USA

<sup>5</sup>Division of Geological and Planetary Sciences, California Institute of Technology, 1200 East California Boulevard, Pasadena, CA 91125, USA

<sup>6</sup>Research Center for the Early Universe (RESCEU), Graduate School of Science, The University of Tokyo, 7-3-1 Hongo, Bunkyo-ku, Tokyo 113-0033, Japan

Received 2018 December 31; revised 2019 April 4; accepted 2019 April 8; published 2019 April 26

## Abstract

Some of the exoplanets observed thus far show featureless or flat transmission spectra, possibly indicating the existence of clouds and/or haze in their atmospheres. Thanks to its large aperture size and broad wavelength coverage, the *James Webb Space Telescope* (*JWST*) is expected to enable a detailed investigation of exoplanet atmospheres, which could provide important constraints on the atmospheric composition obscured by clouds/haze. Here, we use four warm ( $\lesssim 1000$  K) planets suitable for atmospheric characterization via transmission spectroscopy, GJ 1214b, GJ 436b, HD 97658b, and Kepler-51b, as examples to explore molecular absorption features detectable by *JWST* even in the existence of hydrocarbon haze in the atmospheres. We simulate photochemistry, the growth of hydrocarbon haze particles, and transmission spectra for the atmospheres of these four planets. We find that among the planetary parameters considered, super-Earths with hazy, relatively hydrogen-rich atmospheres are mostly expected to produce detectable molecular absorption features such as a quite prominent CH<sub>4</sub> feature at 3.3  $\mu\text{m}$ , even for the extreme case of the most efficient production of photochemical haze. For a planet that has extremely low gravity, such as Kepler-51b, haze particles grow significantly large in the upper atmosphere due to the small sedimentation velocity, resulting in the featureless or flat transmission spectrum in a wide wavelength range. This investigation shows that, in most cases, the transmission spectra with muted features measured by *Hubble Space Telescope* do not preclude strong features at the longer wavelengths accessible by *JWST*.

**Key words:** planets and satellites: atmospheres – planets and satellites: composition – planets and satellites: individual (GJ 1214b, GJ 436b, HD 97658b, and Kepler-51b)

## 1. Introduction

Transmission spectra of close-in exoplanets observed thus far are somewhat diverse (Sing et al. 2016). Some studies have explored such diversity by examining the correlation between the observed amplitude of absorption features and planetary properties (Heng 2016; Stevenson 2016; Crossfield & Kreidberg 2017). All of these studies reached the conclusion that molecular absorption features are less pronounced in transmission spectra for lower equilibrium temperatures, although other planetary properties may affect such a correlation.

One explanation for this correlation is the existence of photochemically produced hydrocarbon haze obscuring the molecular features in the atmospheres of cooler planets (Zahnle et al. 2009; Miller-Ricci Kempton et al. 2012; Morley et al. 2013, 2015). This is because its primary source CH<sub>4</sub> exists only at such low temperatures ( $\lesssim 1000$  K) (e.g., Burrows & Sharp 1999).

Among stars hosting currently observable warm ( $\lesssim 1000$  K) low-mass planets, GJ 1214, GJ 436, and HD 97658 are the only three host stars whose ultraviolet (UV) emission spectra have been observed (France et al. 2016; Loyd et al. 2016; Youngblood et al. 2016). Also, high-precision transmission spectra for their planets were observed with the *Hubble Space Telescope* (*HST*; e.g., Knutson et al. 2014a, 2014b; Kreidberg et al. 2014). They all show flat or featureless transmission

spectra between 1.1 and 1.7  $\mu\text{m}$ , possibly indicating the existence of haze in the atmospheres. Because the knowledge of host-star's UV spectrum is essential for the modeling of hydrocarbon haze (e.g., Kawashima & Ikoma 2018, 2019), the above three planets serve as the most promising targets to understand the nature of haze in exoplanet atmospheres. In addition, Kepler-51b is attracting attention as a favorable target for atmospheric characterization via transmission spectroscopy due to its extremely low density and large atmospheric scale height (Masuda 2014). In terms of haze science, this planet is also an interesting target because the sedimentation velocity of the particles in the atmosphere is expected to be quite low due to its low gravity, which allows particle growth in the upper atmosphere and mute features in the transmission spectrum. Recently, Wang & Dai (2019) investigated the effect of dusty outflows for Kepler-51b and 51d and showed that the existence of small dust of a fixed size at high altitudes could flatten the transmission spectra.

Currently, the number of exoplanets suitable for atmospheric characterization is still small due to the lack of bright targets and sufficient observational precision. Fortunately, the *Transiting Exoplanet Survey Satellite* (*TESS*; Ricker et al. 2014) is expected to detect a great number of transiting exoplanets around nearby stars bright enough for atmospheric characterization. Also, the *James Webb Space Telescope* (*JWST*; Gardner et al. 2006) will enable high-precision transmission

spectroscopy thanks to its large diameter, and also enable the spectroscopy at longer wavelengths than *HST* with its suite of spectroscopy instruments up to  $12\ \mu\text{m}$ , with photometry up to  $28.5\ \mu\text{m}$  (Beichman et al. 2014).

In this Letter, we use the above four favorable planets, GJ 1214b, GJ 436b, HD 97658b, and Kepler-51b, as examples and explore molecular absorption features detectable by *JWST* in the existence of hydrocarbon haze in their atmospheres. Planets similar in size to GJ 1214b and HD 97658b have been shown to be abundant (Fulton & Petigura 2018), indicating more planets in this size range will be found by *TESS* and will be the primary targets for atmospheric characterization by *JWST* (Louie et al. 2018). We describe the models in Section 2, and show the results in Section 3. We discuss several effects to be examined in Section 4, and conclude this Letter in Section 5.

## 2. Method

We model transmission spectra of an atmosphere with hydrocarbon haze using the photochemical, particle growth, and transmission spectrum models of Kawashima & Ikoma (2018) as follows: we first perform photochemical calculations to derive the steady-state distribution of gaseous species. Our reaction rate list is the reduced version of Hu et al. (2012) and we include the reverse reactions in the same way as Hu & Seager (2014). Then we assume that the production rate of haze monomers at each altitude as the sum of the photodissociation rates of the major hydrocarbons in our photochemical model,  $\text{CH}_4$ ,  $\text{HCN}$ , and  $\text{C}_2\text{H}_2$ , as an upper limit for the monomer production rate, as this approach effectively assumes 100% conversion efficiency from the photodissociation of these hydrocarbons to haze monomers. With this assumption, we derive the steady-state distribution of haze particles by the particle growth calculations. Finally, we model transmission spectra of the atmospheres with the obtained distributions of haze particles and gaseous species. For the details of each of the three models, see Kawashima & Ikoma (2018).

As for the UV spectra of the host stars GJ 1214, GJ 436, and HD 97658, we use the data constructed by the MUSCLES Treasury Survey (France et al. 2016; Loyd et al. 2016; Youngblood et al. 2016). As for Kepler-51, whose UV spectrum has not been observed because of its similar properties to the Sun, we use the solar spectrum from Segura et al. (2003).<sup>7</sup>

The setting for the atmospheres is as follows. We assume that the elemental abundance ratios of the atmospheric gas are the solar system ones, which we take from Table 2 of Lodders (2003). For the temperature–pressure profile, we use the analytical formula of Equation (29) of Guillot (2010). We choose the values of the parameters, namely, the intrinsic temperature  $T_{\text{int}}$ , irradiation temperature  $T_{\text{irr}}$ , averaged opacity in the optical  $k_v$  and that in the infrared  $k_{\text{th}}$ , so as to match the temperature–pressure profiles from Miller-Ricci & Fortney (2010; the version with the solar metallicity and efficient dayside-to-nightside heat redistribution) for GJ 1214b and from Lewis et al. (2010; their solar-metallicity version) for GJ 436b. As for HD 97658b and Kepler-51b, we adopt the same parameter values as the case of GJ 1214b except for  $T_{\text{irr}}$ , which we calculate with Equation (1) of Guillot (2010). We adopt the lower-boundary pressure of 1000 bar for

photochemical calculation, while 10 bar in particle growth and transmission spectrum calculations.

For the calculations of photochemistry and particle growth, we choose the values of the reference radius equivalent to 1000 bar so as to roughly match the observed transit radii for a clear solar-composition atmosphere. For Kepler-51b only, we use different values of the 1000 bar radius for two cases of the hazy and clear atmospheres. This is because, with the same 1000 bar radius as in the clear atmosphere case, we would obtain transit radii that are too large for the hazy atmosphere to be consistent with the observed depth due to its extremely low gravity. When calculating the transmission spectra, we find the appropriate value of 10 bar radius that minimizes the reduced  $\chi^2$  value in comparison between the theoretical and observed transit depths. We consider the observed transmission spectra of Kreidberg et al. (2014) and Knutson et al. (2014a, 2014b) for GJ 1214b, GJ 436b, and HD 97658b, respectively, and the observed radius of Kepler-51b from Masuda (2014). For the calculation of theoretical transit depth for each observed data point, we consider the transmission curve of the filter used in the observation, taking those data from the Spanish Virtual Observatory (SVO) Filter Profile Service<sup>8</sup> (Rodrigo et al. 2012; Rodrigo & Solano 2013).

The parameters and their values we use are listed in Table 1.

## 3. Results

Figure 1 shows the transmission spectrum models for atmospheres with and without haze for the cases of GJ 1214b, GJ 436b, HD 97658b, and Kepler-51b. We calculate the deviation in transit depth caused by  $nH_{\text{ref}}$  at a reference pressure level,  $R_{\text{ref}}$ , as  $2nR_{\text{ref}}H_{\text{ref}}/R_s^2$  (Brown 2001), where  $H_{\text{ref}}$  is the atmospheric scale height at  $R_{\text{ref}}$ . The reference pressures are taken to be  $10^{-4}$  bar for GJ 1214b, GJ 436b, and HD 97658b, and  $10^{-6}$  bar for Kepler-51b, which roughly correspond to the pressure levels of the transit radii. Note that the transmission spectrum models for clear atmospheres are also calculated with the distribution of gaseous species from photochemical calculations.

A number of spectral features are produced by molecules above the optically thick photochemical haze. These features are generally  $\lesssim 2$  atmospheric scale heights for GJ 1214b- and GJ 436b-like planets, and  $\lesssim 1$  for HD 97658b-like planets, while  $\lesssim 6$  for the cases of clear atmospheres. As photodissociation is the driver for haze formation, this finding is general for exoplanets having solar composition atmospheres under similar levels of UV irradiation.

Considering a precision of  $\sim 25$  ppm expected to be achieved by *JWST* (Beichman et al. 2014) and a spectral resolution of  $R = 100$ , we find detectable absorption features with the upper-limit production rate of haze monomers for each planet as listed in Table 2.

Some molecular absorption features will be detectable for a planet like GJ 1214b, due to lower incoming UV flux, namely lower monomer production rate, and larger planet-to-star radius ratio. For the planet GJ 1214b itself, however, the  $1.4\ \mu\text{m}$   $\text{H}_2\text{O}$  feature was not detected by Kreidberg et al. (2014) at the precision of  $\sim 25$  ppm. While Morley et al. (2015) demonstrated that their haze formation efficiency parameters of  $\gtrsim 10\%$  could match the observed flatness of Kreidberg et al. (2014) for  $50\times$  Solar atmosphere, by considering particle growth we have

<sup>7</sup> [http://vpl.astro.washington.edu/spectra/stellar/other\\_stars.htm](http://vpl.astro.washington.edu/spectra/stellar/other_stars.htm)

<sup>8</sup> <http://svo2.cab.inta-csic.es/theory/fps/>

**Table 1**  
Model Parameters and Their Values Used in the Simulations

Parameter	Description	Value	References
Common parameters			
$K_{zz}$	Eddy diffusion coefficient	$1.00 \times 10^7 \text{ cm}^2 \text{ s}^{-1}$	
$s_1$	Monomer radius	$1.00 \times 10^{-3} \mu\text{m}$	
$\rho_p$	Particle internal density	$1.00 \text{ g cm}^{-3}$	
GJ 1214b			
$R_s$	Host star radius	$0.201 R_\odot$	Anglada-Escudé et al. (2013)
$M_p$	Planet mass	$6.26 M_\oplus$	Anglada-Escudé et al. (2013)
$R_{1000 \text{ bar}}$	1000 bar radius	$2.07 R_\oplus$	
$a$	Semimajor axis	$0.0148 \text{ au}$	Anglada-Escudé et al. (2013)
$d$	Distance	$14.6 \text{ pc}$	Youngblood et al. (2016)
$T_{\text{int}}$	Intrinsic temperature	$120 \text{ K}$	
$T_{\text{irr}}$	Irradiation temperature	$790 \text{ K}$	
$k_v$	Averaged opacity in the optical	$10^{-4.1} \text{ cm}^2 \text{ g}^{-1}$	
$k_{\text{th}}$	Averaged opacity in the infrared	$10^{-2.7} \text{ cm}^2 \text{ g}^{-1}$	
GJ 436b			
$R_s$	Host star radius	$0.464 R_\odot$	Torres et al. (2008)
$M_p$	Planet mass	$23.2 M_\oplus$	Torres et al. (2008)
$R_{1000 \text{ bar}}$	1000 bar radius	$3.758 R_\oplus$	
$a$	Semimajor axis	$0.02872 \text{ au}$	Torres et al. (2008)
$d$	Distance	$10.1 \text{ pc}$	Youngblood et al. (2016)
$T_{\text{int}}$	Intrinsic temperature	$170 \text{ K}$	
$T_{\text{irr}}$	Irradiation temperature	$860 \text{ K}$	
$k_v$	Averaged opacity in the optical	$10^{-3.6} \text{ cm}^2 \text{ g}^{-1}$	
$k_{\text{th}}$	Averaged opacity in the infrared	$10^{-2.3} \text{ cm}^2 \text{ g}^{-1}$	
HD 97658b			
$R_s$	Host star radius	$0.703 R_\odot$	Dragomir et al. (2013)
$M_p$	Planet mass	$7.86 M_\oplus$	Dragomir et al. (2013)
$R_{1000 \text{ bar}}$	1000 bar radius	$1.943 R_\oplus$	
$a$	Semimajor axis	$0.0796 \text{ au}$	Dragomir et al. (2013)
$d$	Distance	$21.1 \text{ pc}$	Youngblood et al. (2016)
$T_{\text{int}}$	Intrinsic temperature	$120 \text{ K}$	
$T_{\text{irr}}$	Irradiation temperature	$1037 \text{ K}$	
$k_v$	Averaged opacity in the optical	$10^{-4.1} \text{ cm}^2 \text{ g}^{-1}$	
$k_{\text{th}}$	Averaged opacity in the infrared	$10^{-2.7} \text{ cm}^2 \text{ g}^{-1}$	
Kepler-51b			
$R_s$	Host star radius	$0.940 R_\odot$	NASA Exoplanet Archive <sup>a</sup>
$M_p$	Planet mass	$2.1 M_\oplus$	Masuda (2014)
$R_{1000 \text{ bar}}$	1000 bar radius	$1.8 R_\oplus$ <sup>b</sup>	
$a$	Semimajor axis	$0.2514 \text{ au}$	Masuda (2014)
$T_{\text{int}}$	Intrinsic temperature	$120 \text{ K}$	
$T_{\text{irr}}$	Irradiation temperature	$793 \text{ K}$	
$k_v$	Averaged opacity in the optical	$10^{-4.1} \text{ cm}^2 \text{ g}^{-1}$	
$k_{\text{th}}$	Averaged opacity in the infrared	$10^{-2.7} \text{ cm}^2 \text{ g}^{-1}$	

**Notes.**

<sup>a</sup> <https://exoplanetarchive.ipac.caltech.edu>

<sup>b</sup> We use the value of  $2.3 R_\oplus$  for the clear atmosphere case.

confirmed that our 1, 10, 100, 1000× Solar atmospheres all fail to become as flat as the observation, even adopting the maximum monomer production rates (Kawashima & Ikoma 2019). This possibly indicates extremely high metallicity, and/or aggregate haze particles (Adams et al. 2019), and/or coexistence of haze and other aerosols (see also the discussion in Section 4). The message here is that a GJ 1214b-like planet, with a solar composition atmosphere and similar UV environment, will be particularly suitable for future atmospheric characterization. In the case of HD 97658b, all of the features in the wavelength range are undetectable due

to the higher incoming UV flux, namely a higher monomer production rate and a smaller planet-to-star radius ratio.

Among the detectable molecules, it is promising that several features of CH<sub>4</sub>, which is a key indicator of haze formation, remains detectable even in the existence of haze for GJ 1214b- and GJ 436b-like planets, especially for its 3.3 μm feature. Note that this strong 3.3 μm CH<sub>4</sub> feature has been detected in the solar occultation spectrum of cooler celestial bodies in our solar system such as Saturn (Dalba et al. 2015) and Titan (Robinson et al. 2014). In the spectrum for Kepler-51b, the CH<sub>4</sub> features are invisible, because CH<sub>4</sub> is photodissociated

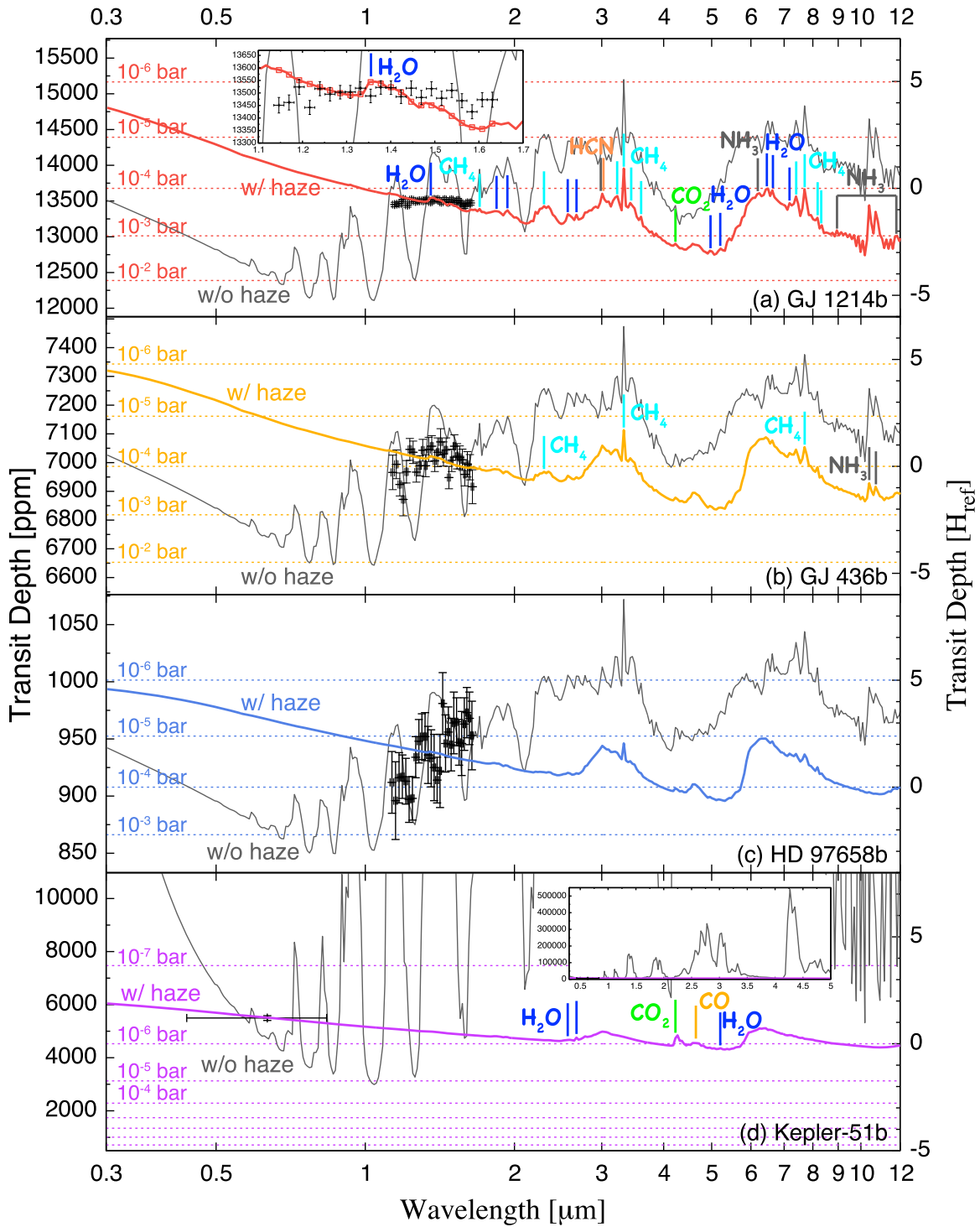


**Figure 1.** Transmission spectrum models for atmospheres with haze (thick color lines) and without haze (thin gray lines) for the cases of GJ 1214b (a), GJ 436b (b), HD 97658b (c), and Kepler-51b (d). This is in the order of the assumed total haze monomer production rate throughout the atmosphere, from the lowest panel to the highest panel, and reflects the amount of UV flux each planet receives. Those values are  $1.38 \times 10^{-12}$ ,  $7.83 \times 10^{-12}$ ,  $5.45 \times 10^{-11}$ , and  $1.17 \times 10^{-10} \text{ g cm}^{-2} \text{ s}^{-1}$  for GJ 1214b, GJ 436b, HD 97658b, and Kepler-51b, respectively. The left vertical axes show the transit depths in ppm, while the right ones show those in atmospheric scale height at a certain pressure level for the hazy atmosphere cases (see the text for details). Horizontal dotted lines represent the transit depths corresponding to the pressure levels of every one order for the hazy atmosphere cases (see Equation (67) of Kawashima & Ikoma 2018). Additionally, zoomed-in and zoomed-out views are shown for GJ 1214b (a) and Kepler-51b (d), respectively. Observed transmission spectra of Kreidberg et al. (2014), Knutson et al. (2014a), and Knutson et al. (2014b) for GJ 1214b, GJ 436b, HD 97658b, respectively, and the observed radius of Kepler-51b from Masuda (2014) are also plotted with black points for reference. Note that horizontal error bars are the bandpasses or the FWHM of those used. The red points in the zoomed-in view for GJ 1214b (a) show the models binned at the observed bandpasses. The transmission spectrum models are smoothed with the spectral resolution of  $R = 100$ . Note the broad bumps at 3.0, 4.6, and 6.3  $\mu\text{m}$  come from the absorption features of the tholin-like haze particles (Khare et al. 1984).



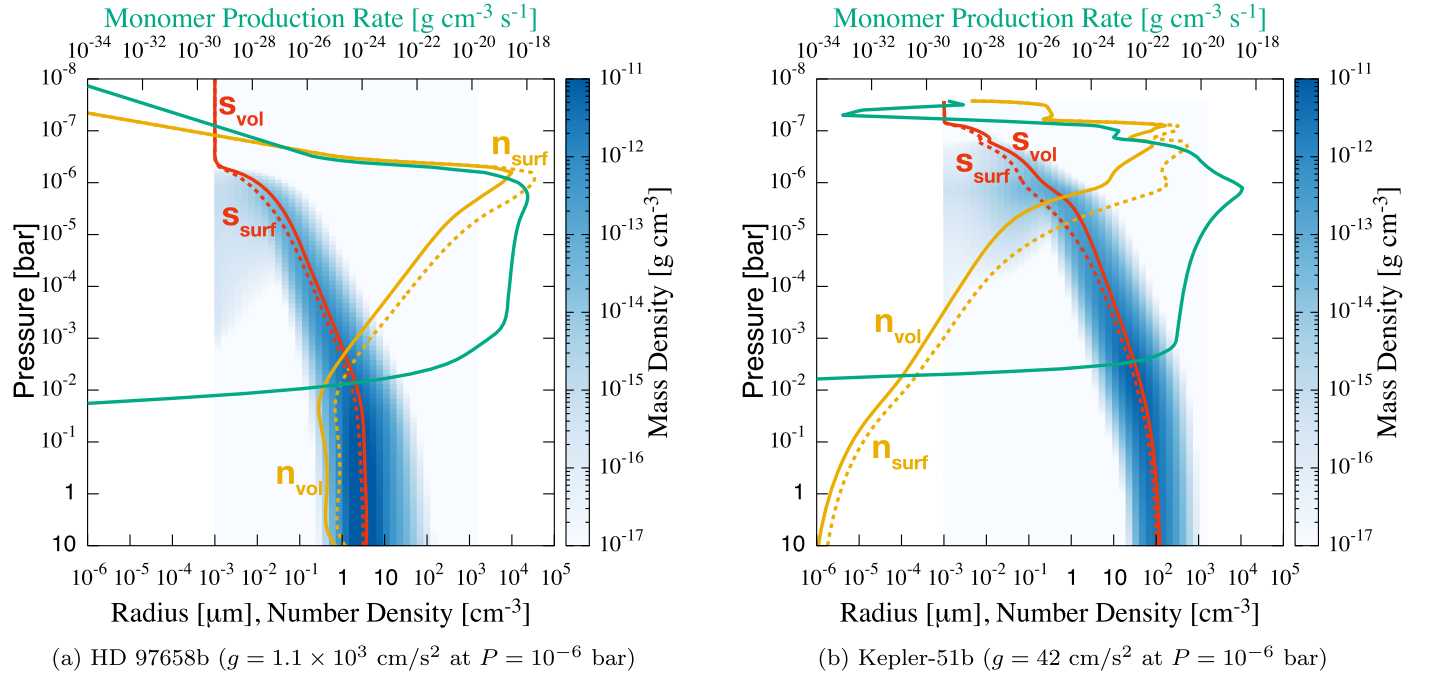


**Figure 2.** Vertical profiles of the properties of haze particles including the volume-average radius  $s_{\text{vol}}$  (solid red line) and number density  $n_{\text{vol}}$  (solid orange line), and the surface-average radius  $s_{\text{surf}}$  (dashed red line) and number density  $n_{\text{surf}}$  (dashed orange line), along with that of the monomer mass production rate (solid green line) for the cases of (a) HD 97658b and (b) Kepler-51b. See Kawashima & Ikoma (2018) for the definition of each quantity. The mass densities for all the size bins at each pressure level are also plotted with the blue contour.

**Table 2**  
Detectable Absorption Features by *JWST*

Planet Type	Molecules	Wavelength ( $\mu\text{m}$ )
GJ 1214b	H <sub>2</sub> O	1.4, 1.8, 1.9, 2.6, 2.7, 5.0, 5.2, 6.5, 6.6, 7.2
	CH <sub>4</sub>	1.7, 2.3, 3.2, 3.3, 3.4, 3.6, 7.4, 7.7, 8.2, 8.3
	NH <sub>3</sub>	3.0, 6.2, 8.9–11.8
	HCN	3.0
	CO <sub>2</sub>	4.2
GJ 436b	CH <sub>4</sub>	2.3, 3.3, 7.7
	NH <sub>3</sub>	10.4, 10.7
HD 97658b	...	...
Kepler-51b	H <sub>2</sub> O	2.6, 2.7, 5.2
	CO <sub>2</sub>	4.3
	CO	4.6

and virtually absent above a thick haze layer at the low pressures of  $\sim 10^{-6}$  bar.

In the case of Kepler-51b, the transmission spectrum model for the atmosphere with haze is quite featureless due to the existence of large haze particles in the upper atmosphere, unlike in the other three cases. However, distinct absorption features of CO<sub>2</sub> and CO are detectable due to their larger abundances in the upper atmosphere. This comes from its extremely low gravity, which makes an optical depth for a given pressure much larger and thus both the photodissociation rate of CH<sub>4</sub> and resultant production flux of atomic carbon much smaller. This very small production flux of C allows effective conversion of C into CO/CO<sub>2</sub> by reaction between H<sub>2</sub>O, while C remains abundant and CO/CO<sub>2</sub> less abundant for the other planet cases.

In Figure 2, we plot the calculated vertical profiles of haze properties for the typical super-Earth gravity case of

(a) HD 97658b and the extremely low gravity case of (b) Kepler-51b. In the case of HD 97658b, particles do not grow large in the upper atmosphere ( $\lesssim 10^{-6}$  bar) because sedimentation occurs faster than collisional growth. Collisional growth occurs significantly from the pressure level of  $\sim 10^{-6}$  bar on, and results in haze particles with the average radius of  $\sim 3\text{--}4 \mu\text{m}$  at the lower boundary of 10 bar. On the other hand, in the case of Kepler-51b haze particles grow much larger in the upper atmosphere ( $\sim 0.1 \mu\text{m}$  at  $\sim 10^{-6}$  bar) and results in particles as large as  $\sim 100 \mu\text{m}$  at 10 bar. This is because particles can become large via collisional growth even in the upper atmosphere, instead of falling downward rapidly due to the small sedimentation velocity from low gravity. Note that although the monomer production rate for Kepler-51b is  $\sim 2$  times higher than that for HD 97658b, the effect of the extremely low gravity makes a much greater contribution to such a difference between those two spectra than that of high monomer production rate. Trends of vertical profiles for GJ 1214b and GJ 436b are similar to that of HD 97658b, but with slightly smaller haze mass density because of the smaller monomer production rates (see Kawashima & Ikoma 2018, for the dependence on monomer production rate).

#### 4. Discussion

In this study, we have assumed the maximum production rate of haze monomers in order to explore the detectable features at the worst case for solar composition atmospheres. As for the eddy diffusion coefficient, the molecular absorption features become more prominent for the larger value because of the efficient downward transport of haze particles, while they remain similar for the smaller value (Kawashima & Ikoma 2019).

In order to briefly assess the effect of metallicity and C/O ratio, in Figure 3 we show the transmission spectrum models

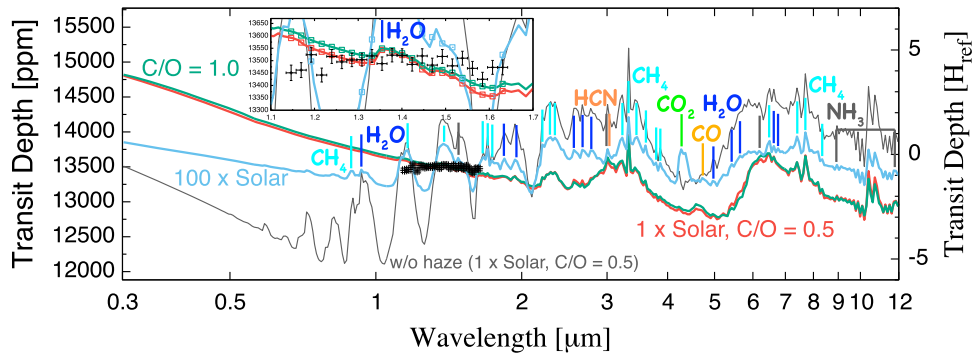


**Figure 3.** Same as Figure 1(a) but transmission spectrum models for the cases of  $100\times$  Solar (light blue line) and  $C/O = 1.0$  (green line) atmospheres are also plotted. Detectable molecular absorption features for the case of  $100\times$  Solar atmosphere are labeled.

for the cases of different metallicities and  $C/O$  ratios for GJ 1214b. More absorption features become detectable for the case of  $100\times$  Solar atmosphere because of the smaller monomer production rate due to an enhanced photon-shielding effect by other molecules, while some features at relatively long wavelengths become undetectable due to smaller atmospheric scale height (Kawashima & Ikoma 2019). On the other hand, the effect of the  $C/O$  ratio is relatively small and, among the detectable features for the solar composition atmosphere,  $H_2O$  features at 1.8, 5.0, 5.2, and  $7.2\ \mu\text{m}$ ,  $CO_2$  features at  $4.2\ \mu\text{m}$ , and  $NH_3$  features at  $6.2\ \mu\text{m}$  become undetectable due to the slightly higher monomer production rate (Kawashima & Ikoma 2019).

In addition to hydrocarbon haze, the existence of other aerosols can mute spectral features in transmission: condensation clouds such as  $KCl$ ,  $ZnS$ ,  $K_2SO_4$ ,  $ZnO$ , and graphite clouds in the temperature range of interest in this study ( $\lesssim 1000\ \text{K}$ ; Miller-Ricci Kempton et al. 2012; Morley et al. 2013; Mbarek & Kempton 2016; Gao & Benneke 2018; Ohno & Okuzumi 2018; Ormel & Min 2019) and photochemical haze made of sulfur species (Hu et al. 2013; Zahnle et al. 2016; Gao et al. 2017).

In outflowing atmospheres the velocity of the outward flow, while having little effect on the profiles of pressure and density, may affect the sedimentation of small particles. The sedimentation velocity of haze particles is much faster than the outward velocity, which we estimate with the isothermal Parker solution (Parker 1958) for simplicity, for all the cases except Kepler-51b. We have confirmed that in the case of Kepler-51b, the sedimentation velocity of the volume-averaged-size particles is smaller than the outward velocity for the region of the pressures lower than  $1.3 \times 10^{-7}$  bar. However, because the dominant monomer production region is below this pressure level, the flow would have little impact on our results. The detailed consideration of this effect is beyond the scope of this study.

As for extended atmospheres like that of Kepler-51b, the effect of the tidal potential may affect the hydrostatic structure of the atmosphere. By using Equation (12) of Erkaev et al. (2007), we have confirmed that the gravitational potential at the optically thick radius at  $1.0 \times 10^{-6}$  bar, which is 9% of its Hill radius, would decrease to 86% due to the tidal potential and thus do not have significant impact on our results.

## 5. Conclusions

In this study, we have used four warm ( $\lesssim 1000\ \text{K}$ ) planets suitable for atmospheric characterization via transmission

spectroscopy, GJ 1214b, GJ 436b, HD 97658b, and Kepler-51b, as examples and explored molecular absorption features detectable by *JWST* even in the existence of hydrocarbon haze in their atmospheres. Using the models of Kawashima & Ikoma (2018), we have simulated photochemistry, the growth of hydrocarbon haze particles, and transmission spectra for the atmospheres of these four planets.

We have found that among the planetary parameters considered, super-Earths with hazy, relatively hydrogen-rich atmospheres are mostly expected to produce detectable molecular absorption features such as a quite prominent  $CH_4$  feature at  $3.3\ \mu\text{m}$ , even for the extreme case of the most efficient production of photochemical haze. The sizes of those features correspond to  $1 \sim 2$  atmospheric scale heights; while they are substantially smaller than a haze-free atmosphere, those features would be detectable with at precision expected for *JWST*. In particular, planets with higher gravity, lower UV irradiation, and higher temperature are more suitable (Kawashima & Ikoma 2019). A slight disagreement between our synthetic spectrum and the very flat one observed for GJ 1214b, however, implies the importance of additional confounding effects.

We have also demonstrated that in the case of the extremely low gravity planet Kepler-51b, haze particles grow significantly larger in the upper atmosphere due to the small sedimentation velocity, resulting in the featureless or flat transmission spectrum in a wide wavelength range.

In summary, various molecular absorption features are expected to be detectable for relatively hydrogen-rich atmospheres, even in the existence of hydrocarbon haze with *JWST*, given its high-precision and long-wavelength capabilities. We thus suggest that the transmission spectra with muted features measured by *HST* in most cases do not preclude strong features at the longer wavelengths accessible by *JWST*.

We thank the anonymous referee for a careful reading and constructive comments, which helped us improve this Letter greatly. The research was carried out at the Jet Propulsion Laboratory, California Institute of Technology, under a contract with the National Aeronautics and Space Administration. Y.K. thanks the travel support of JPL's Science Visitor and Colloquium Program. Y.K. is supported by the Grant-in-Aid for JSPS Fellow (JSPS KAKENHI No. 15J08463), Leading Graduate Course for Frontiers of Mathematical Sciences and Physics, Grant-in-Aid for Scientific Research (A) (JSPS KAKENHI No. 15H02065), and the European Union's Horizon 2020 Research and Innovation Programme under Grant Agreement 776403. R.H. is supported by NASA

grant No. 80NM0018F0612. M.I. is supported by JSPS KAKENHI No. 18H05439 and Core-to-Core Program International Network of Planetary Sciences. This work has made use of the MUSCLES Treasury Survey High-Level Science Products (doi:10.17909/T9DG6F) and the SVO Filter Profile Service (<http://svo2.cab.inta-csic.es/theory/fps/>) supported from the Spanish MINECO through grant AyA2014-55216.

### ORCID iDs

Yui Kawashima  <https://orcid.org/0000-0003-3800-7518>

Masahiro Ikoma  <https://orcid.org/0000-0002-5658-5971>

### References

- Adams, D., Gao, P., de Pater, I., & Morley, C. 2019, *ApJ*, 874, 61
- Anglada-Escudé, G., Rojas-Ayala, B., Boss, A. P., Weinberger, A. J., & Lloyd, J. P. 2013, *A&A*, 551, A48
- Beichman, C., Benneke, B., Knutson, H., et al. 2014, *PASP*, 126, 1134
- Brown, T. M. 2001, *ApJ*, 553, 1006
- Burrows, A., & Sharp, C. M. 1999, *ApJ*, 512, 843
- Crossfield, I. J. M., & Kreidberg, L. 2017, *AJ*, 154, 261
- Dalba, P. A., Muirhead, P. S., Fortney, J. J., et al. 2015, *ApJ*, 814, 154
- Dragomir, D., Matthews, J. M., Eastman, J. D., et al. 2013, *ApJL*, 772, L2
- Erkaev, N. V., Kulikov, Y. N., Lammer, H., et al. 2007, *A&A*, 472, 329
- France, K., Parke Loyd, R. O., Youngblood, A., et al. 2016, *ApJ*, 820, 89
- Fulton, B. J., & Petigura, E. A. 2018, *AJ*, 156, 264
- Gao, P., & Benneke, B. 2018, *ApJ*, 863, 165
- Gao, P., Marley, M. S., Zahnle, K., Robinson, T. D., & Lewis, N. K. 2017, *AJ*, 153, 139
- Gardner, J. P., Mather, J. C., Clampin, M., et al. 2006, *SSRv*, 123, 485
- Guillot, T. 2010, *A&A*, 520, A27
- Heng, K. 2016, *ApJL*, 826, L16
- Hu, R., & Seager, S. 2014, *ApJ*, 784, 63
- Hu, R., Seager, S., & Bains, W. 2012, *ApJ*, 761, 166
- Hu, R., Seager, S., & Bains, W. 2013, *ApJ*, 769, 6
- Kawashima, Y., & Ikoma, M. 2018, *ApJ*, 853, 7
- Kawashima, Y., & Ikoma, M. 2019, *ApJ*, in press
- Khare, B. N., Sagan, C., Arakawa, E. T., et al. 1984, *Icar*, 60, 127
- Knutson, H. A., Benneke, B., Deming, D., & Homeier, D. 2014a, *Natur*, 505, 66
- Knutson, H. A., Dragomir, D., Kreidberg, L., et al. 2014b, *ApJ*, 794, 155
- Kreidberg, L., Bean, J. L., Désert, J.-M., et al. 2014, *Natur*, 505, 69
- Lewis, N. K., Showman, A. P., Fortney, J. J., et al. 2010, *ApJ*, 720, 344
- Lodders, K. 2003, *ApJ*, 591, 1220
- Louie, D. R., Deming, D., Albert, L., et al. 2018, *PASP*, 130, 044401
- Loyd, R. O. P., France, K., Youngblood, A., et al. 2016, *ApJ*, 824, 102
- Masuda, K. 2014, *ApJ*, 783, 53
- Mbarek, R., & Kempton, E. M.-R. 2016, *ApJ*, 827, 121
- Miller-Ricci, E., & Fortney, J. J. 2010, *ApJL*, 716, L74
- Miller-Ricci Kempton, E., Zahnle, K., & Fortney, J. J. 2012, *ApJ*, 745, 3
- Morley, C. V., Fortney, J. J., Kempton, E. M.-R., et al. 2013, *ApJ*, 775, 33
- Morley, C. V., Fortney, J. J., Marley, M. S., et al. 2015, *ApJ*, 815, 110
- Ohno, K., & Okuzumi, S. 2018, *ApJ*, 859, 34
- Ormel, C. W., & Min, M. 2019, *A&A*, 622, A121
- Parker, E. N. 1958, *ApJ*, 128, 664
- Ricker, G. R., Winn, J. N., Vanderspek, R., et al. 2014, *Proc. SPIE*, 9143, 914320
- Robinson, T. D., Maltagliati, L., Marley, M. S., & Fortney, J. J. 2014, *PNAS*, 111, 9042
- Rodrigo, C., & Solano, E. 2013, IVOA Note 2013 May 10, Filter Profile Service Access Protocol Version 1.0, <http://ivoa.net/documents/Notes/SVOFPSDAL/index.html>
- Rodrigo, C., Solano, E., & Bayo, A. 2012, IVOA Working Draft 2012 October 15, SVO Filter Profile Service Version 1.0
- Segura, A., Krelove, K., Kasting, J. F., et al. 2003, *AsBio*, 3, 689
- Sing, D. K., Fortney, J. J., Nikolov, N., et al. 2016, *Natur*, 529, 59
- Stevenson, K. B. 2016, *ApJL*, 817, L16
- Torres, G., Winn, J. N., & Holman, M. J. 2008, *ApJ*, 677, 1324
- Wang, L., & Dai, F. 2019, *ApJL*, 873, L1
- Youngblood, A., France, K., Parke Loyd, R. O., et al. 2016, *ApJ*, 824, 101
- Zahnle, K., Marley, M. S., & Fortney, J. J. 2009, arXiv:0911.0728
- Zahnle, K., Marley, M. S., Morley, C. V., & Moses, J. I. 2016, *ApJ*, 824, 137